Applied Physics Letters ARTICLE pubs.aip.org/aip/apl

Impact of threading dislocations on the V-defect assisted lateral carrier injection and recombination in InGaN quantum well LEDs

Cite as: Appl. Phys. Lett. **126**, 211104 (2025); doi: 10.1063/5.0271165
Submitted: 15 March 2025 · Accepted: 16 May 2025 ·
Published Online: 29 May 2025

Rinat Yapparov,[1] Alejandro Quevedo,[2] Tanay Tak,[3] Shuji Nakamura,[2,3] Steven P. DenBaars,[2,3] James S. Speck,[3] and Saulius Marcinkevičius[1,a)]

AFFILIATIONS

[1]Department of Applied Physics, KTH Royal Institute of Technology, AlbaNova University Center, 10691 Stockholm, Sweden
[2]Electrical and Computer Engineering Department, University of California, Santa Barbara, California 93106, USA
[3]Materials Department, University of California, Santa Barbara, California 93106, USA

[a)]Author to whom correspondence should be addressed: sm@kth.se

ABSTRACT

The nonuniform hole distribution between InGaN quantum wells (QWs) of light emitting diodes (LEDs) has a negative impact on LED efficiency. The uniformity can be increased by using lateral hole injection through sidewalls of V-defects, which form at threading dislocations. However, the inherent coupling between the V-defects and dislocations might affect efficiency of the hole injection and nonradiative recombination. In this work, we have tested the possible impact of the dislocations on the injection and recombination by means of scanning near-field electroluminescence and photoluminescence spectroscopy on single green-emitting InGaN QW LEDs containing large (~0.5 μm) V-defects. The measurements have not provided any evidence of a lower hole injection efficiency or enhanced nonradiative recombination at the dislocations located at the V-defect facets or their apexes. This shows that large V-defects are excellent volumetric injectors for long wavelength InGaN LEDs. Furthermore, it was established that V-defects are preferential hole injectors even in single quantum well devices. Compared to vertical injection, the V-defect injection allows lowering the operating voltage, which should contribute to an enhanced wall plug efficiency.

The active region of visible wavelength GaN-based light emitting diodes (LEDs) is based on multiple InGaN quantum wells (QWs). To assure effective LED operation with a minimal impact of the nonradiative Shockley–Read–Hall (SRH) and Auger–Meitner recombination, all QWs should be populated by electrons and holes at similar concentrations. The primary hindrance in achieving the uniform carrier distribution is the interwell hole transport because the large hole effective mass and high $In_xGa_{1-x}N$/GaN quantum confinement and polarization barriers make the interwell hole transfer slow and inefficient.[1–4]

Hole injection through semipolar QWs located on the facets of V-defects has recently emerged as a novel volumetric carrier injection mechanism,[5] which allows circumventing the poor hole injection by the direct thermionic transport. The V-defects form at threading dislocations (TDs) under conditions of kinetically limited growth and have shapes of inverted hexagonal pyramids with semipolar $\{10\bar{1}1\}$ sidewall planes.[6] Long wavelength LEDs with the V-defect injection have demonstrated high wall plug efficiencies of 20%–30%.[7] Recent investigations of multiple QW LEDs have shown that the V-defects are preferential sites for the hole injection with most of the hole current flowing through the V-defects rather than directly from the *p*-GaN to the QWs.[8,9]

However, the inherent coupling between the V-defects and TDs raises a question whether introduction of the V-defects does not increase the SRH recombination because TDs in GaN structures are often considered to be efficient nonradiative recombination centers.[10–16] Moreover, it has been shown that the TDs do not terminate at the apex of the V-defect (because dislocations cannot terminate within the crystal) but may proceed to the surface on one of the V-defect facets.[17] Thus, TDs might affect not only the SRH recombination in the QWs[18] but also the hole injection because of their recombination during the sidewall QW transport.[17] In this work, we have examined these issues by mapping electroluminescence (EL) and

photoluminescence (PL) in V-defect LEDs. We have addressed two questions: (i) do TDs located on the facets of the V-defects influence the hole injection and (ii) do the TDs on the V-defect facets and at their apexes affect recombination in the polar QWs. LEDs with large V-defects with a diameter of about 0.5–0.6 μm have been studied because the large defects ensure a larger lateral injection area and higher potential barrier between the polar QWs and TDs.[19,20] In addition, they are expected to reveal finer details in the EL and PL maps.

The studied single QW LEDs were grown by metalorganic chemical vapor deposition on double side polished *c*-plane sapphire substrate. Starting from the substrate, an LED contains 2 μm unintentionally doped (UID) and 3 μm *n*-doped GaN layers, a 25 nm low temperature (LT) grown GaN layer that nucleates the V-defects, 40 period GaN/$In_{0.05}Ga_{0.95}N$ superlattice (SL) that further enlarges the V-defects, 200 nm (sample A) or 350 nm (sample B) UID GaN layer, 0.5 nm pre-QW GaN layer, single 2.5 nm $In_xGa_{1-x}N$ QW capped by 3 nm of $Al_{0.30}Ga_{0.70}N$, 10 nm GaN barrier, 10 nm *p*-$Al_{0.20}Ga_{0.80}N$ electron blocking layer (EBL), and 85 nm *p* and p^+ GaN contact layers. The different thicknesses of the post-SL UID GaN layer produced V-defects of a different diameter: ~0.5 μm for sample A and ~0.6 μm for sample B. The top metal contact of Pd/Au (50/100 nm) with a honeycomb pattern of open 20-μm diameter circular apertures provides areas for the near-field measurements of the device. The measurements were conducted with the LEDs on wafer using needle probes to apply bias.

Maps of EL and PL spectra, and PL decay times were taken at room temperature using a multimode scanning near-field optical microscope (SNOM).[21] The scans were performed at a constant distance between the sample and the fiber probe, which was mounted on a quartz tuning fork. The surface topography maps were taken using shear force feedback between the sample and the probe.[22] The probes were manufactured from a multimode silica fiber by HF etching and Al coating. The apex of the probe was cut by a focused ion beam milling, which opened an aperture of ~100 nm in diameter and produced a sharp edge for the surface topography scan. EL spectra were measured by collecting emission through the probe. PL was measured in the illumination-collection (IC) mode with both excitation and PL collection taking place through the probe. Scans from 2×2 to 6×6 μm^2 were performed. The spatial resolution in planar regions is typically determined by the aperture diameter; however, because of the significant distance (108 nm) between the device surface and the QW, the resolution was lower, ~200 nm. Maps of different spectral parameters were extracted after EL or PL spectra were recorded at each position of a scan. The spectra were measured with a spectrometer with a liquid N_2 cooled charge coupled device detector. PL excitation was performed directly into the QW with 2nd harmonic pulses from a Ti:sapphire laser (the pulse duration is 200 fs, the central wavelength is 390 nm, and the repetition frequency is 4 MHz). PL transients were measured with a time-correlated single photon counter with a temporal response of 50 ps. For the PL decay time maps, the times were determined by fitting the initial part of the PL decay by a single exponential. Most of the EL maps were measured at the bias voltage of 3.3 V and current of 10 mA. Assuming a uniform current distribution across the device, this corresponds to the current density of 10 A/cm^2. Additional measurements in the voltage (current) range from 3.0 V (3 mA) to 3.5 V (20 mA) produced qualitatively similar maps. Most of the PL scans were taken at the voltage of the EL threshold, 2.6 V (current 0.3 mA).

Figure 1(a) shows a plane view scanning electron microscopy image of sample B. In addition to the large V defects that nucleate in the LT GaN layer, one can notice smaller V-defects that originate in the QW and do not serve as hole injectors.[17] Figure 1(b) displays a schematic of our LED structure in the V-defect region, showing a TD on one of the facets, which is typical for structures with unfilled V-defects.[17]

Figure 2 presents maps of the surface topography and EL intensity for devices A and B. One can notice an EL intensity increase at positions of the large V-defects. As will be shown later, PL intensity does not experience a corresponding enhancement. This indicates that the spatial nonuniformity of the EL maps is caused by the preferential injection through the V-defect facets rather than enhancement of the light extraction. The latter, according to the Monte–Carlo calculations, does not exceed 45%.[23] Previously, the preferential hole injection via the V-defects has been demonstrated in multiple QW LEDs.[8,9,24] Current results show that even in single QW devices, the hole injection takes place mainly through the V-defects despite that the QW is adjacent to the *p*-side of the structure. This indirect hole injection path [Fig. 1(b)] is aided by the lower potential height, smaller thickness, and smaller polarization discontinuity of the AlGaN EBL at the semipolar compared to polar QWs.[25] The preferential hole injection through the V-defects shows that even a single green-emitting QW has a large polarization barrier for the vertical hole injection. The V-defect hole injection would require a lower operating voltage potentially increasing the wall plug efficiency compared to the vertical hole injection.

In this work, we focus on the impact of the TDs on the hole injection and nonradiative carrier recombination. The influence of the TD segment located on the V-defect facet can be assessed from the shape of the large EL intensity regions around the V-defects shown in Fig. 2 and, on a finer scale, in Fig. 3. Before we proceed to the discussion on the hole trapping during transport through the semipolar QW, let us examine the EL intensity maps in the V-defect regions. One can notice that even though the V-defect facet dimensions are considerably larger than the spatial resolution of the experiment, shapes of the strong EL regions lack fine details. This can be understood considering geometry of the experiment. In planar parts of the device, the near-field EL polarization is mostly perpendicular to the probe axis, and EL couples into the probe primarily through the aperture.[26] In the V-defects, the experimental configuration is different. First, the distance between the probe aperture and sample surface increases since the relatively large

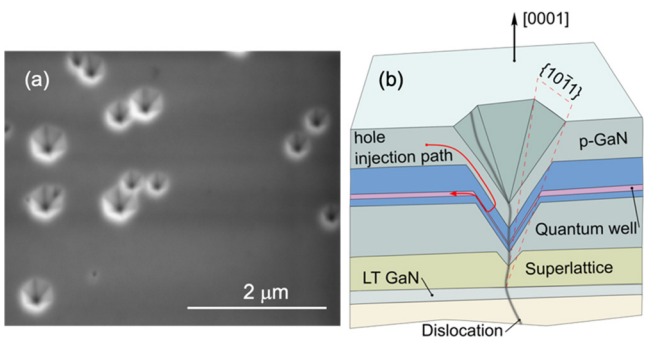

FIG. 1. Scanning electron microscopy image of the device surface (a); schematics of the LED cross section in the V-defect region (b). The red arrow shows the hole path via the semipolar sidewall QW.

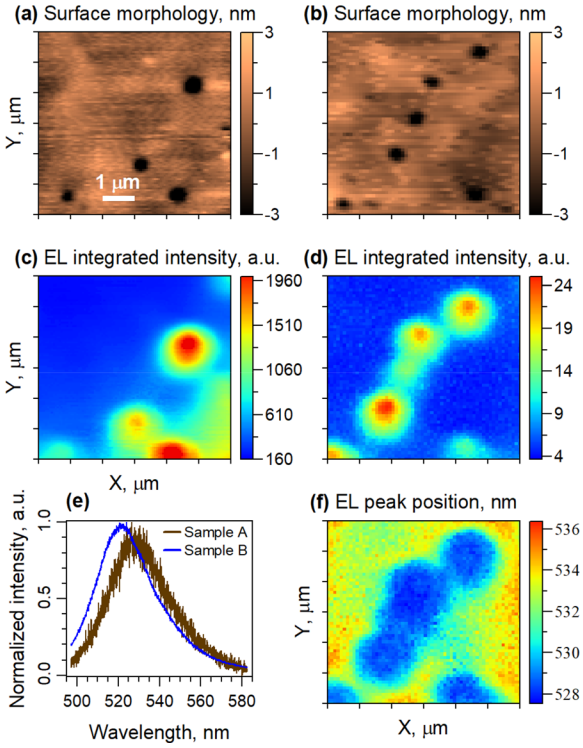

FIG. 2. $6 \times 6\ \mu m^2$ maps of the surface topography (a) and (b) and spectrally integrated EL intensity (c) and (d) for the devices B (a) and (c) and A (b) and (d). (e) Typical near-field spectra of devices A and B and (f) peak wavelength map of device A.

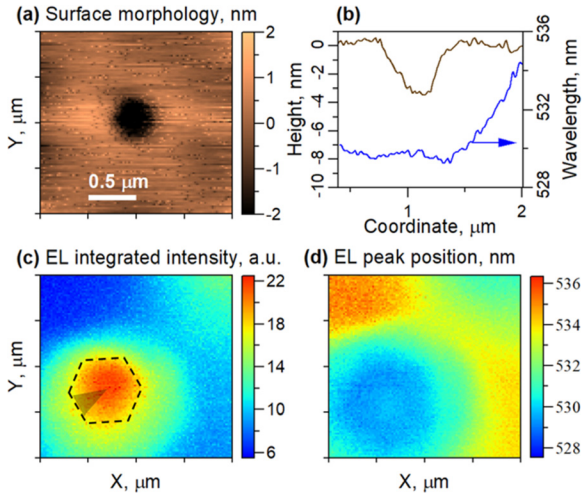

FIG. 3. $2 \times 2\ \mu m^2$ maps of the surface topography (a), spectrally integrated EL intensity (c), and peak wavelength (d) of device A. (b) Cross section profiles of the topography and the peak wavelength taken over the center of the V-defect. The height profile does not reflect the whole depth of the V-defect because of the large SNOM probe thickness. The shaded area in (c) schematically shows the area that would be affected if the hole injection was hindered by the TD.

probe cannot maintain the same distance to the sample surface within the V-defect. This should reduce the near-field coupling between the QW and probe aperture. On the other hand, more light couples into the probe via metalized edges because of excitation of surface plasmons in the metal coating.[26] This coupling is enhanced by the lighting rod effect for the EL polarization parallel to the probe axis.[27] As can be judged from the featureless PL intensity maps discussed (Fig. 4), these effects compensate each other, and the nonplanarity of the sample surface does not affect the mapped luminescence intensity. The same effect has previously been observed for multiple QW LEDs.[8] On the other hand, the increased role of the metalized probe edges should deteriorate the spatial resolution since not only the probe aperture but also the whole probe pick up the near-field signal. This explains why the V-defect areas in the EL intensity maps lack detail. In spite of that, the impact on the TD on the hole transport can still be assessed. The key feature here is that the shapes of the high EL intensity regions are nearly circularly symmetric with no obvious intensity reduction on one of the sides. This is an indication that the hole injection takes place with similar efficiency through all the facets of the V-defect, even the one containing the TD. In the opposite case, one would expect a reduced emission intensity from one side of the V-defect, as schematically shown in Fig. 3(c). The absence of the locally reduced hole injection indicates that eventual hole traps in the TD region do not affect the hole injection. Most likely, this occurs because the traps under the positive bias are filled.

The increased near-field coupling between the regions of the polar QW surrounding the V-defect and the near-field probe explains another peculiar feature, namely, the maximum of the EL intensity in the center of the V-defect where the polar QW has a void. In the QW regions around the V-defect, the injected carrier concentration is high, and emission is strong. In the V-defect center, the near-field probe picks up the signal from all sides around the V-defect. These contributions sum up producing strong EL even though that area has an opening in the polar QW.

Additional information on the near-field emission may be obtained from the peak wavelength maps. Overall, in the V-defect areas, the peak wavelength experiences a slight blue shift [Fig. 2(f)] caused by the local band filling and electric field screening in the areas of the high carrier concentration around the V-defects. Interestingly, in the small area scan ($2 \times 2\ \mu m^2$, Fig. 3), the overall blue shift in the V-defect area is followed by a small red shift in the center [Figs. 3(b) and 3(d)]. Following the discussion presented earlier, the central part should contain contributions from all sides of the V-defect and originate from regions close to the polar QW edges. It has been shown[17,28] that within several tens of nm from the TD, the indium content in the polar QW is larger, and the bandgap is smaller than further away in the structure; hence, emission from that part of the well would experience a red shift.

The presented discussion shows that the TDs at the V-defect facets do not deteriorate efficiency of the hole injection through the V-defects. The second question raised in the introduction is whether the TD at the V-defect facet and apex affects efficiency of the polar QW emission. Figure 4 shows spectrally integrated PL intensity maps for carrier excitation into the QW of the LED biased to the EL emission threshold (2.6 V). One can notice that the PL maps do not correlate with the map of the surface topography. The absence of reduced intensity areas at the V-defect sidewalls shows that the TDs located on

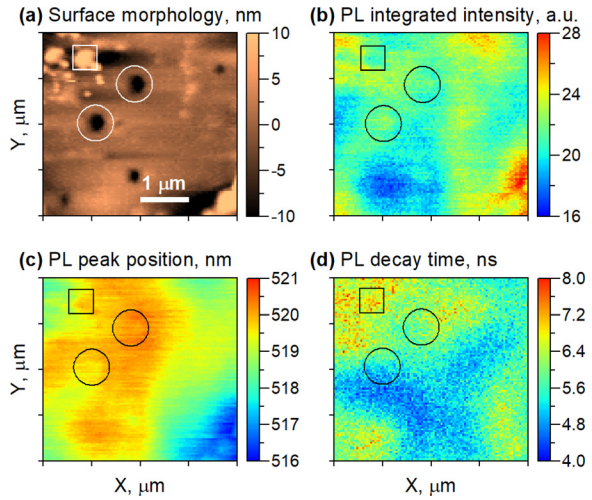

FIG. 4. $4 \times 4\ \mu m^2$ maps of the surface topography (a), spectrally integrated PL intensity (b), peak wavelength (c), and PL decay time (d) for device B. A square surface impurity marker at the top left corners allows an exact superposition of the topography and optical maps. Positions of the V-defects are indicated by ring markers.

the sidewalls do not affect the recombination rate in the polar QW. In a way, this is expected since TDs are separated from the polar QW by the semipolar QW and ∼30 nm of the EBL and *p*-GaN. The absence of the low intensity areas at the V-defects also shows that for the optical excitation of the polar QWs, the TD at the V-defect apex does not induce an enhanced SRH recombination either. A weak influence of TDs on the emission properties of green InGaN QW LEDs has also been observed in Ref. 29.

Thus, PL maps neither reveal any clear features that would suggest an enhanced SRH recombination at the TDs nor indicate of an enhanced light extraction at the V-defects. However, the PL intensity is an integral parameter, which depends not only on the rate of the nonradiative but also on the radiative recombination.[21] A more direct way to explore the spatial distribution of the SRH recombination is by mapping PL decay times. The decay times map [Fig. 4(d)] does not reveal an enhanced SRH recombination at the V-defects either, which shows that the SRH recombination rate in the TD areas is not enhanced.

Considering mechanisms that prevent the SRH recombination at TDs, one should examine several effects. The first one is filling of the TD-related electron and hole traps. Once the traps are filled, the nonradiative SRH recombination proceeds at a relatively low rate, which, in high quality long wavelength unbiased InGaN QWs, is $\sim 1 \times 10^7\ s^{-1}$.[30] The other mechanism is related to the potential barriers of the semipolar QWs preventing carriers from polar QWs to reach TD-related traps, as shown by Hangleiter *et al.*[19] Our EL and PL measurements allow distinguishing conditions at which each of these mechanisms is most relevant. In the EL experiment, the LED is under positive bias, and electrons and holes in the *n* and *p* GaN layers are in direct vicinity of the TD and can be trapped. However, the carrier concentration under the LED operating conditions is high, and the traps are easily filled.[31] Once the traps are filled, holes injected from the *p* region quickly (∼20 ps) pass the semipolar QW and end up in the polar QW, where they are isolated from the TD-related traps by the high potential barriers of the semipolar QWs and semipolar EBL.

In the case of the optical carrier excitation directly into the polar QW, at positive bias, the TD-related traps are filled. However, at zero and negative bias, they might be empty. When changing the bias from 3 to −3 V, we did not observe any qualitative changes in the PL intensity or lifetime maps (not shown), just some lifetime shortening due to the carrier sweep-out from the QWs. No selective lifetime reduction in the V-defect regions at the negative bias took place. This allows concluding that once carriers are in the polar well, their transfer to the TD-related traps or SRH centers is inhibited by the semipolar QW and EBL potential barriers. Thus, the traps are most relevant for the carrier capture directly from the *p* and *n* GaN layers at low currents before the traps are filled. For carriers in the polar QW, the dominating mechanism preventing carrier capture to the TD-related traps is their isolation by the potential barriers.

In conclusion, scanning near-field optical spectroscopy of EL and PL has been used to study the impact of TDs on the hole injection and SRH recombination in single InGaN QW LEDs containing large V-defects. The measurements have not provided any evidence of a lower hole injection efficiency or enhanced nonradiative recombination at the TDs on the V-defect facets or apexes. The lack of the reduced hole injection suggests that eventual hole traps in the dislocation region under the positive bias are filled. Concerning the recombination, the absence of the enhanced SRH recombination can be assigned to potential barriers formed by the semipolar sidewall QWs and the EBL in the region of the V-defects. Furthermore, our results show that even for single QW LEDs, the hole injection via the V-defects is the preferential hole injection path compared to the vertical transport allowing to circumvent polarization barriers on the *p*-side of the structure, reduce the operating voltage, and, potentially, increase the wall plug efficiency.

The research at KTH has been financially supported by the Swedish Energy Agency (Project No. P2022-00251) and the Swedish Research Council (Project No. 2023-03538). Support at UCSB was provided by the Solid State Lighting and Energy Electronics Center (SSLEEC), U.S. Department of Energy under the Office of Energy Efficiency & Renewable Energy (EERE) Award Nos. DE-EE0009691, the National Science Foundation (NSF) RAISE program (Grant No. DMS-1839077), and the Simons Foundation (Grant No. 601952 for J.S.S.); T.T. acknowledges the Department of Defense's National Defense Science and Engineering Graduate Fellowship for their support.

AUTHOR DECLARATIONS

Conflict of Interest

The authors have no conflicts to disclose.

Author Contributions

Rinat Yapparov: Data curation (lead); Formal analysis (equal); Investigation (lead); Methodology (equal); Visualization (lead); Writing – review & editing (supporting). **Alejandro Quevedo:** Data curation (supporting); Investigation (supporting); Methodology (equal); Resources (equal); Visualization (supporting); Writing – review & editing (supporting). **Tanay Tak:** Data curation (supporting); Investigation (supporting); Methodology (equal); Resources (equal);

Visualization (supporting); Writing – review & editing (supporting). **Shuji Nakamura:** Resources (equal). **Steven P. DenBaars:** Resources (equal); Supervision (equal). **James S. Speck:** Conceptualization (supporting); Funding acquisition (equal); Resources (equal); Supervision (equal); Writing – review & editing (supporting). **Saulius Marcinkevičius:** Conceptualization (lead); Formal analysis (equal); Funding acquisition (equal); Investigation (supporting); Supervision (equal); Visualization (supporting); Writing – original draft (lead); Writing – review & editing (lead).

DATA AVAILABILITY

The data that support the findings of this study are available from the corresponding author upon reasonable request.

REFERENCES

[1]A. David, M. J. Grundmann, J. F. Kaeding, N. F. Gardner, T. G. Mihopoulos, and M. R. Krames, Appl. Phys. Lett. **92**, 053502 (2008).
[2]J. P. Liu, J.-H. Ryou, R. D. Dupuis, J. Han, G. D. Shen, and H. B. Wang, Appl. Phys. Lett. **93**, 021102 (2008).
[3]W. G. Scheibenzuber and U. T. Schwarz, Appl. Phys. Express **5**, 042103 (2012).
[4]S. Marcinkevičius, R. Yapparov, L. Y. Kuritzky, Y.-R. Wu, S. Nakamura, S. P. DenBaars, and J. S. Speck, Appl. Phys. Lett. **114**, 151103 (2019).
[5]Z. Quan, L. Wang, C. Zheng, J. Liu, and F. Jiang, J. Appl. Phys. **116**, 183107 (2014).
[6]X. H. Wu, C. R. Elsass, A. Abare, M. Mack, S. Keller, P. M. Petroff, S. P. DenBaars, J. S. Speck, and S. J. Rosner, Appl. Phys. Lett. **72**, 692 (1998).
[7]F. Jiang, J. Zhang, L. Xu, J. Ding, G. Wang, X. Wu, X. Wang, C. Mo, Z. Quan, X. Guo, C. Zheng, S. Pan, and J. Liu, Photonics Res. **7**, 144 (2019).
[8]Y. Li, W. Tang, Y. Zhang, M. Guo, Q. Li, X. Su, A. Li, and F. Yun, Nanomaterials **9**, 633 (2019).
[9]R. Yapparov, T. Tak, J. Ewing, F. Wu, S. Nakamura, S. P. DenBaars, J. S. Speck, and S. Marcinkevičius, Appl. Phys. Lett. **125**, 031108 (2024).
[10]M. H. Zoellner, G. A. Chahine, L. Lahourcade, C. Mounir, C. L. Manganelli, T. U. Schülli, U. T. Schwarz, R. Zeisel, and T. Schroeder, ACS Appl. Mater. Interfaces **11**, 22834 (2019).
[11]S. Kurai, S. Higaki, N. Imura, K. Okawa, R. Makio, N. Okada, K. Tadatomo, and Y. Yamada, Phys. Status Solidi (b) **225**, 1700358 (2018).
[12]J. Bruckbauer, P. R. Edwards, T. Wang, and R. W. Martin, Appl. Phys. Lett. **98**, 141908 (2011).
[13]M. Yoshikawa, M. Murakami, H. Ishida, and H. Harima, Appl. Phys. Lett. **94**, 131908 (2009).
[14]T. Meyer, M. Peter, J. Danhof, U. T. Schwarz, and B. Hahn, Phys. Status Solidi (a) **208**, 1523 (2011).
[15]S. J. Henley and D. Cherns, J. Appl. Phys. **93**, 3934 (2003).
[16]E. B. Yakimov, A. Y. Polyakov, I.-H. Lee, and S. J. Pearton, J. Appl. Phys. **123**, 161543 (2018).
[17]F. Wu, J. Ewing, C. Lynsky, M. Iza, S. Nakamura, S. P. DenBaars, and J. S. Speck, J. Appl. Phys. **133**, 035703 (2023).
[18]C.-H. Ho, J. S. Speck, C. Weisbuch, and Y.-R. Wu, Phys. Rev. Appl. **17**, 014033 (2022).
[19]A. Hangleiter, F. Hitzel, C. Netzel, D. Fuhrmann, U. Rossow, G. Ade, and P. Hinze, Phys. Rev. Lett. **95**, 127402 (2005).
[20]N. Okada, H. Kashihara, K. Sugimoto, Y. Yamada, and K. Tadatomo, J. Appl. Phys. **117**, 025708 (2015).
[21]M. Mensi, R. Ivanov, T. K. Uždavinys, K. M. Kelchner, S. Nakamura, S. P. DenBaars, J. S. Speck, and S. Marcinkevičius, ACS Photonics **5**, 528 (2018).
[22]E. Betzig, P. L. Finn, and J. S. Weiner, Appl. Phys. Lett. **60**, 2484 (1992).
[23]M. S. Wang and X.-J. Huang, Chin. Phys. B **22**, 086803 (2013).
[24]R. Yapparov, T. Tak, J. Ewing, S. Nakamura, S. P. DenBaars, J. S. Speck, and S. Marcinkevičius, J. Appl. Phys. **136**, 083103 (2024).
[25]A. E. Romanov, T. J. Baker, S. Nakamura, and J. S. Speck, J. Appl. Phys. **100**, 023522 (2006).
[26]*Handbook of Nano-Optics and Nanophotonics*, edited by M. Ohtsu (Springer, Berlin, 2013), pp. 1–1068.
[27]H. W. Kihm, K. G. Lee, D. S. Kim, and K. J. Ahn, Opt. Commun. **282**, 2442 (2009).
[28]Y. Yamaguchi, Y. Kanitani, Y. Kudo, J. Uzuhashi, T. Ohkubo, K. Hono, and S. Tomiya, Nano Lett. **22**, 6930 (2022).
[29]K. Zhang, C. Hu, V. G. T. Vangipuram, L. Meng, C. Chae, M. Zhu, J. Hwang, K. Kash, and H. Zhao, J. Vac. Sci. Technol. B **41**, 062207 (2023).
[30]S. Marcinkevičius, R. Yapparov, Y. C. Chow, C. Lynsky, S. Nakamura, S. P. DenBaars, and J. S. Speck, Appl. Phys. Lett. **119**, 071102 (2021).
[31]S. Marcinkevičius, T. Tak, Y. C. Chow, F. Wu, R. Yapparov, S. P. DenBaars, S. Nakamura, and J. S. Speck, Appl. Phys. Lett. **124**, 181108 (2024).